

Article

Phenylamine/Amide Grafted in Silica as Sensing Nanocomposites for the Removal of Carbamazepine: A DFT Approach

Manuel Algarra ^{1,*}, Shehdeh Jodeh ^{2,*}, Israa Aqel ², Ghadir Hanbali ², Smail Radi ³, Said Tighadouini ⁴, Raed Alkowni ⁵, Juan Soto ⁶, Subhi Samhan ⁷, Savaş Kaya ⁸ and Konstantin P. Katin ⁹

- ¹ Department of Science, INAMAT² Institute for Advanced Materials and Mathematics, Campus of Arrosadia, Public University of Navarra, 31006 Pamplona, Spain
 - ² Department of Chemistry, An-Najah National University, Nablus P.O. Box 7, Palestine; israa.aqel90@gmail.com (I.A.); g.hanbali@najah.edu (G.H.)
 - ³ Faculty of Sciences Oujda, Mohammed First University, LCAE, BP 717, Oujda 60000, Morocco; s.radi@ump.ac.ma
 - ⁴ Laboratoire de Synthèse Organique, Extraction et Valorisation, Faculté des Sciences Ain-Chock, Université Hassan II Casablanca, Casablanca 20100, Morocco; tighadouinis@gmail.com
 - ⁵ Department of Biology and Biotechnology, An-Najah National University, Nablus P.O. Box. 7, Palestine; ralkowni@najah.edu
 - ⁶ Department of Physical Chemistry, Faculty of Science, Campus de Teatinos, University of Málaga, 29071 Málaga, Spain; soto@uma.es
 - ⁷ Research and Development Center, Palestine Water Authority, Ramallah 2174, Palestine; subhisamhan@pwa.ps
 - ⁸ Department of Pharmacy, Health Services Vocational School, Sivas Cumhuriyet University, Sivas 58140, Turkey; savaskaya@cumhuriyet.tr
 - ⁹ Department of Condensed Matter Physics, National Research Nuclear University “MEPhI”, 115409 Moscow, Russia; KPKatin@yandex.ru
- * Correspondence: manuel.algarra@unavarra.es (M.A.); sjodeh@najah.edu (S.J.)



Citation: Algarra, M.; Jodeh, S.; Aqel, I.; Hanbali, G.; Radi, S.; Tighadouini, S.; Alkowni, R.; Soto, J.; Samhan, S.; Kaya, S.; et al. Phenylamine/Amide Grafted in Silica as Sensing Nanocomposites for the Removal of Carbamazepine: A DFT Approach. *Chemosensors* **2022**, *10*, 76. <https://doi.org/10.3390/chemosensors10020076>

Academic Editor: Daniele Merli

Received: 31 December 2021

Accepted: 7 February 2022

Published: 11 February 2022

Publisher's Note: MDPI stays neutral with regard to jurisdictional claims in published maps and institutional affiliations.



Copyright: © 2022 by the authors. Licensee MDPI, Basel, Switzerland. This article is an open access article distributed under the terms and conditions of the Creative Commons Attribution (CC BY) license (<https://creativecommons.org/licenses/by/4.0/>).

Abstract: This study aimed to remove carbamazepine from aqueous solutions, using functional silica phenylamine (SiBN), which is characterized and showed excellent chemical and thermal stability. Adsorbents based on silica were developed due to their unusually large surface area, homogenous pore structure, and well-modified surface properties, as silica sparked tremendous interest. It was determined to develop a novel silica adsorbent including phenylamine and amide (SiBCON). The adsorbents obtained were analyzed by various spectroscopy devices, including SEM, FT-IR and TGA analysis. The maximum removal rates for carbamazepine were 98.37% and 98.22% for SiBN and SiBCON, respectively, when optimized at room temperature, pH 9.0, initial concentration of 10 mg·L⁻¹ and contact time of 15 min. Theoretical tools are widely used in the prediction of the power of interactions between chemical systems. The computed data showed that new amine modified silica is quite effective in terms of the removal of carbamazepine from aqueous solution. Calculation binding energies and DFT data showed that there is a powerful interaction between amine-modified silica and carbamazepine.

Keywords: carbamazepine; amine-modified silica; adsorption; phenylamine; regeneration

1. Introduction

Pharmaceutical companies produce medicines, antibiotics, lipid regulators, etc., which have become used in our daily life for the health treatment of both animals and humans. According to World Health Organization (WHO) in 2017, more than USD 1135 billion was spent on prescription medications [1]. Over the past decades, pharmaceuticals have emerged in aquatic environments as an environmental issue [2].

Among the most used, the antiepileptic drug carbamazepine (CBZ) [3,4], is one of the compounds considered non-biodegradable in the environment, because it is not fully assimilated by humans and it is released to the media, and mainly accumulated in the aquatic system [5]. Due to its high stability, the concentration of CBZ is observed to be more than 12 times greater than that of other pharmacological preparations [6]. The largest source of pharmaceuticals in aquatic ecosystems was discovered to be wastewater treatment plant effluents [7], and this was due to wastewater treatment plants' inability to remove micro contaminants. In wastewater treatment plants, the highest proportion of CBZ removal was 65.6% [8,9]. As a result, the discharge of effluents from wastewater treatment plants into the environment might result in the formation of micropollutants [10]. To minimize micropollutants in surface waters, adequate post-treatment is required. There are several technological treatments to deal with this concern, because CBZ was classified as a potentially harmful compound for aquatic organisms by Council Directive 92/32/EEC [11]. Extraction models were used for this aim; water-soluble proteins extracted from *Moringa stenopetala* seeds were used for the extraction of non-steroidal anti-inflammatory drugs (NSAIDs) and CBZ drugs in pharmaceutical wastewaters [12]. Nanoparticles obtained from hematite were used to remove CBZ [13]. Remediation, which involves the transformation of this pollutant to non-toxic levels, offers advantages over the conventional remediation methods. Metal-organic frameworks (MOFs) were compared with a commercial activated carbon (F400) to remove CBZ from aqueous solution, showing a removal performance of up to 85% [14].

Wastewater passed through a granulated activated carbon and treated by means of the Fenton reaction resulted in an overall CBZ removal of 99.5% [15]. To obtain a total removal of CBZ, the Fenton reaction was performed together with a flexible bifunctional nano-electrocatalytic textile material, $\text{Fe}_3\text{O}_4\text{-NP@CNF}$, and the mineralization of CBZ was completed in water [16]. Conventional ozonation was used to transform CBZ into oxalic and formic acid [17]; when supported by NiO, it was sufficient to remove it completely to be mineralized [18]. Photodegradation of CBZ by a solar/ Cl_2 /carbon nitride system demonstrated a considerable degradation of carbamazepine, as high as 97.8%, which was more than twice that of the solar/ Cl_2 system (43.8%) [19,20].

Adsorbents are considered an alternative to all techniques previously described, because they are low cost and easy to use and have demonstrated no risk to humans, and pollutants are retained on the adsorbent surface because they are not released to the environment. Adsorbents based on silica structure have been proposed to remove diclofenac and CBZ by hexagonal mesoporous silicate, and were proposed with immobilized amine and mercaptan functional groups on their surface; the results improved when compared with the homologous mesoporous silicates Santa Barbara Amorphous-15 (SBA-15) and MCM-41, when tested together with powdered activated carbon [21]. The success of these materials is based on their high porosity, an ordered structure of pores correlated with the high volume, which improves their adsorption capacity. Additionally, the easiest surface functionalization, based on the high-density presence of organosilane functional groups, susceptible to be modified according to the molecules to be trapped [22,23]. These covalently ligand-bonded organic functional groups are usually highly stable and resistant to removal from the surface using organic solvents or water [24]. To this end, a great number of organic molecules were immobilized on silica gel surface, xylenol orange [25].

The aim of this study is to study the remediation of CBZ by an amine-based silica gel from aqueous solution and supported by theoretical studies.

2. Materials and Methods

2.1. Chemicals

Silica gel, with an average pore diameter of 60 and particle size ranging from 72 to 233 mesh, was activated by heating at 165 °C (24 h). (3-amino) propyltrimethoxysilane (APTMS, 97%) and carbamazepine (CBZ, 99.9%) were purchased from Janssen Chim-

ica without further purification. Stock solutions of CBZ ($50 \text{ mg}\cdot\text{L}^{-1}$) were prepared in Milli Q water.

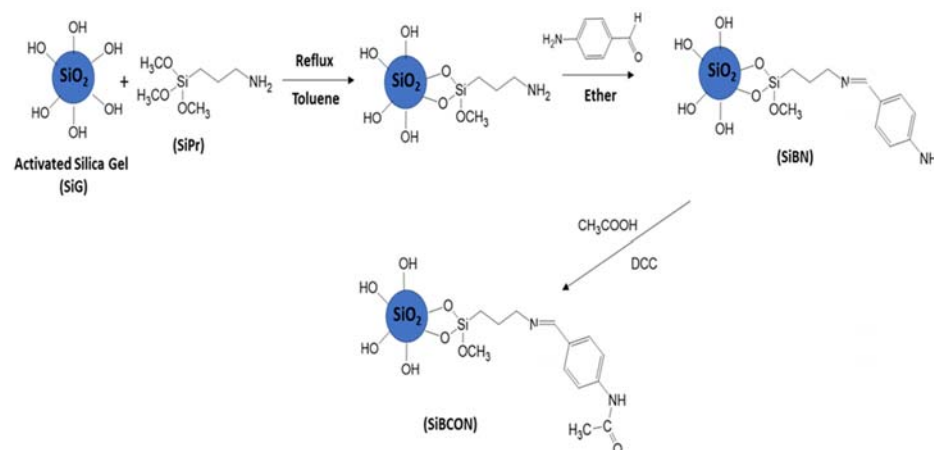
2.2. Preparation of Phenyl-Amide-Substituted Silica

2.2.1. Preparation of Silica-Gel-Immobilized Propylamine (SiPr)

APTMS in the presence of dry toluene interacts with activated silica gel (SiG) to generate amino groups linked to the silica surface [26]. 4-Aminobenzaldehyde was subsequently reacted with NH_2 groups on the silica surface (for 12 h at RT), yielding the novel material SiBN using anhydrous diethyl ether as a solvent.

2.2.2. Synthesis of Phenylamine-Substituted Silica

As indicated in Scheme 1, activated silica gel (SiG) (2 g) was treated with APTMS (SiPr) to produce the SiBN adsorbent (0.83 g). The material was washed with toluene to generate amino groups on the surface of SiG. The NH_2 groups on the silica surface were then reacted with 4-aminobenzaldehyde (0.25 g) at RT under moderate circumstances (shaking for 12 h) using anhydrous diethyl ether (100 mL) as the solvent to generate a new SiBN adsorbent [9]. SiBCON nanocomposite was prepared as shown in Scheme 1. Amine (SiBN) (0.09 g) and acid (acetic acid) (0.09 mL) were added to THF (9 mL) at 0°C , and then dicyclohexylcarbodiimide (DCC) (0.18 g) was added. The mixture was left to stir for 48 h at room temperature. Then, the product was taken after two days and washed with a small amount of the following substances: EtOAc, NaHCO_3 , HCl and brine (0.9%). The organic layer was dried with MgSO_4 [27].



Scheme 1. Synthesis of phenylamine-substituted silica.

2.3. Adsorption Experiments

Experiments were carried out using SiBN and SiBCON dosages of 10.0 mg. Here, 10 mL of various initial CBZ concentrations ($5\text{--}50 \text{ mg}\cdot\text{L}^{-1}$) water solutions were added and mechanically stirred at 200 rpm in an orbital incubator (Gallenkamp, model INR-250, Loughborough, Leicestershire, UK). The samples were held at various test temperatures ($25\text{--}55^\circ\text{C}$) for a contact time ranging between 5 and 120 min to achieve the equilibrium. HPLC was used to measure CBZ equilibrium concentrations. The absorbance readings for a variety of known concentrations of CBZ solutions were used to create a calibration curve. At pH levels ranging from 2 to 12, the influence of pH on the amount of CBZ removed was studied. The initial concentrations' pH levels were modified by the addition of NaOH and HCl (0.1M). The following Equations (1) and (2) were used to compute equilibrium concentrations of retained CBZ on the adsorbent phase q_e ($\text{mg}\cdot\text{g}^{-1}$) [28]:

$$q_e = \frac{V(C_0 - C_e)}{W} \quad (1)$$

where C_0 ($\text{mg}\cdot\text{L}^{-1}$) is the metal concentration in the solution prior to treatment, C_e ($\text{mg}\cdot\text{L}^{-1}$) is the metal concentration in the solution following treatment, V (L) is the volume of the solution, and W (g) is the adsorbent dosage. CBZ elimination efficiency was determined using the following formula:

$$\%R = \frac{(C_0 - C_e)}{C_0} * 100 \% \quad (2)$$

2.4. Adsorption Kinetics

To establish the kinetics and rate determination stages, different models were utilized. These models demonstrate the adsorption system's efficacy and the rate of removal of a given component via the usage of a specific adsorbent. Furthermore, it indicates whether the adsorption process is chemical in nature and what stage influences the pace. A pseudo-kinetic first/second model, for example, is a popular example of an adsorption kinematic model. This was the first model designed to describe kinetic energy for the adsorption reaction. The following equations express the pseudo-first-order Equation (3) [29]:

$$\log(q_e - q_t) = \log q_e - \left(\frac{K_1}{2.303} \right) t \quad (3)$$

where q_e and q_t are the quantities of the analyte absorbed ($\text{mg}\cdot\text{g}^{-1}$) and K_1 is the pseudo-first-order rate constant for adsorption (min^{-1}). K_1 may be determined by plotting the values of $\text{Log}(q_e - q_t)$ as the y -axis vs. values of t as the x -axis. This form of kinetic implies that chemical adsorption is the rate-determining phase, which includes valence attraction between the adsorbate and the adsorbent through electronic exchange/sharing. The equation for this kinetic model type is:

$$\frac{t}{q_t} = \frac{1}{q_e} t + \frac{1}{K_2 q_e^2} \quad (4)$$

where K_2 is the rate constant for adsorption pseudo-second-order ($\text{g}\cdot\text{mg}^{-1}\cdot\text{min}^{-1}$). By plotting a linear relationship between the values of t/q_t as the y -axis and values of t as the x -axis, we can derive $(1/K_2 q_e^2)$ from the y -intercept and $(1/q_e)$ which equals the slope of the graph. The intraparticle diffusion model is shown in Equation (5).

$$q_t = K_{id} t^{0.5} + C \quad (5)$$

where C_i is the thickness of the boundary layer and K_{id} is a constant. A plot of q_t vs. $t^{0.5}$ revealed a straight line with a high correlation coefficient (R^2), indicating that the intraparticle diffusion model may be applied to all three types of experimental data. The data fitting using the intra-particle diffusion model shows two different areas, indicating that the diffusion process involves two steps: exterior mass transfer or boundary layer diffusion and intra-particle or micropore diffusion [30].

2.5. Adsorption Isotherms

The isotherm models are useful because they depict the mechanism of interaction between adsorbents and adsorbate. The two most popular models for this purpose are the Langmuir and Freundlich [31,32]. The Langmuir model (Equation (6)) assumes the formation of an adsorbate monolayer on a homogenous surface of an adsorbent:

$$\frac{C_e}{q_e} = \frac{1}{q_m} C_e + \frac{1}{q_m K_L} \quad (6)$$

where C_e denotes the adsorbate concentration at equilibrium ($\text{mg}\cdot\text{L}^{-1}$), q_e denotes the maximal capacity of monolayer coverage ($\text{mg}\cdot\text{g}^{-1}$), and K_L denotes the Langmuir isotherm

constant ($\text{L}\cdot\text{mg}^{-1}$). The Freundlich isotherm is used to describe adsorption on a heterogeneous surface (Equation (7)):

$$\ln q_e = \frac{1}{n} \ln C_e + \ln K_F \quad (7)$$

K_F , on the other hand, is a constant reflecting the adsorbent's capacity ($\text{mg}\cdot\text{g}^{-1}$). n is a coefficient that indicates the preferred adsorption process ($\text{g}\cdot\text{L}^{-1}$), and $1/n$ is an indicator of the adsorption process's favorability. If $1/n$ is $\ll 1$, the adsorption is normal. If ($10 > n > 0$), this contributes to a favorable adsorption process.

2.6. Adsorption Thermodynamics

The thermodynamic study examines enthalpy (ΔH), free energy ΔG , and entropy ΔS . Thermodynamic characteristics are required to determine if the process is spontaneous or not. Gibb's free energy change is an illustration of the spontaneity of a chemical reaction. Gibb's free energy of the process must be calculated using both enthalpy and entropy components, as shown in the van't Hoff equation (Equation (8)). The thermodynamic study was performed by studying enthalpy, free energy, and entropy.

$$\ln K_d = -\frac{\Delta H^\circ}{RT} + \frac{\Delta S^\circ}{R} \quad (8)$$

2.7. FT-IR, TGA, Adsorption and SEM

An infrared spectrophotometer was used to collect FT-IR spectra, and the BET equation was used to determine a specific region of the modified silica. After purifying the material in a stream of dry nitrogen, nitrogen adsorption was obtained using the Thermoquest Sorpsomatic 1990 analyzer. On the TGA Q50 V6.7 Build 203, mass loss measurements were performed with a heating rate of 10°C minimum and $-190:10$ atmospheres of oxygen/nitrogen. Scanning electron microscopy was used to examine the surface morphology of SiBN and SiBCON (SEM, Hitachi S-2600N, 5.0 kV, Ontario, Canada). The solid samples were scattered over adhesive carbon tape that was held in place by metallic disks.

2.8. Computational Details

To evaluate chemical reactivity of carbamazepine and corresponding adsorbents, we applied the conceptual density functional theory (CDFT). CDFT provides a qualitative understanding and quantitative predictions of chemical reactivity through quantum descriptors [33]. Descriptors such as chemical potential (μ), electrophilicity (ω), electronegativity (χ), softness (η), and hardness (η) provide important insights about the stability of the electron-donating and electron-accepting capabilities of chemical systems [34]. Mathematical definitions of the mentioned parameters in CDFT can be understood from the following formulae [35].

$$\mu = -\chi = \left[\frac{\partial E}{\partial N} \right]_{v(r)} = -\left(\frac{I + A}{2} \right) \quad (9)$$

$$\eta = \frac{1}{2} \left[\frac{\partial^2 E}{\partial N^2} \right]_{v(r)} = \frac{I - A}{2} \quad (10)$$

$$\sigma = 1/\eta \quad (11)$$

$$\omega = \mu^2/2\eta = \chi^2/2\eta \quad (12)$$

In the given equations, E , N , I and A represent the total electronic energy, the number of electrons, ground state ionization energy and ground state electron affinity of a chemical system, respectively. According to Koppman formalism [36], the negative values of HOMO and LUMO orbital energies are almost equivalent to ionization energy and electron affinity, respectively. We used density functional theory for theoretical investigations of the non-

covalent interaction of two adsorbents (SiBN and SiBCON) with carbamazepine. In the present study, we used density functional theory for the theoretical investigation of non-covalent interaction of both sensing systems (SiBN and SiBCON) with CBZ [37–39]. All calculations were performed at the B3LYP/6-311G** level of theory with GAMESS-US software. This method is commonly used to describe both carbamazepine [40,41] and silicon nanostructures [42,43]. Dispersion corrections, D3, proposed by Grimme were added. Interacting molecules were placed in water solution, simulated with polarized continuum model (PCM) implemented in GAMESS-US [44,45].

3. Results and Discussion

3.1. Adsorbent Characterization

Nitrogen adsorption and adsorption isotherms were measured at 77 K, and accordingly, the specific surface area of BET for SiBN and SiBCON was calculated using low-temperature nitrogen adsorption/desorption isotherms data based on the absorption data at P/P_0 from 0.05 to 0.2. It has been determined as $2.47 \text{ m}^2 \cdot \text{g}^{-1}$. Pore size and mean pore size were calculated by the BJH model [46]. The pore sizes of SiBN and SiBCON were determined as 2.45×10^{-2} and $2.7 \times 10^{-2} \text{ cm}^3 \cdot \text{g}^{-1}$, respectively. The pore diameter was measured to be 3.5 and 3.64 nm. As a result, SiBN and SiBCON materials with pore sizes ranging from 2 to 50 nm are categorized as porous [47].

3.2. SEM Analysis

SEM images of the modified silica show a rough and enhanced porous character, indicating that the material has a high potential for CBZ use. After activating the pristine SiG (Figure 1A), the reaction with APTMS revealed that it was bound, resulting in a smoothed surface (Figure 1B, a material with a porous structure and a specific functional group on the surface with an irreversibly bound amino group. After reaction with 4-aminobenzalehyde, the morphology of the obtained SiBN microparticles was observed (Figure 1C; 50 μm scale). Additionally, the clear micro/nano structure after reaction with DCC to obtain SiBCON is shown in Figure 1D.

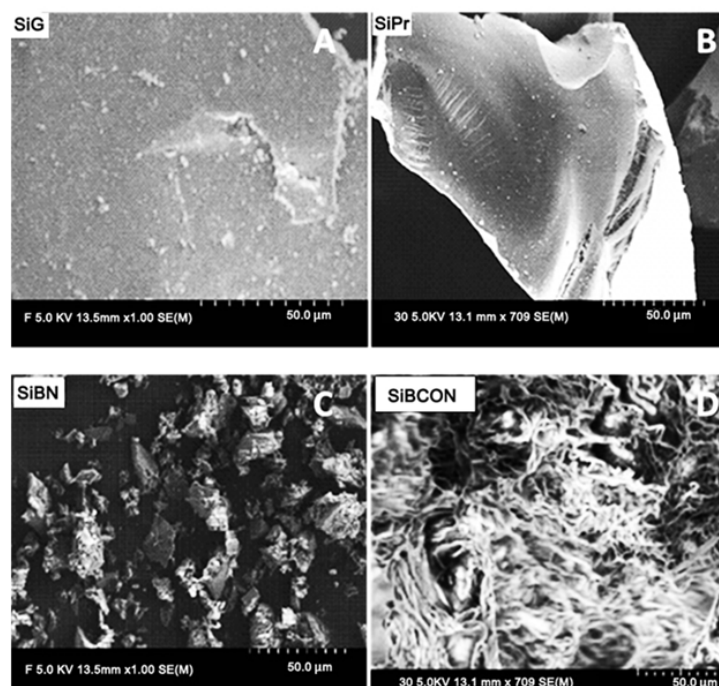


Figure 1. SEM micrographs of (A) activated silica gel (SiG) and the modified silica derivatives (B) SiPr, (C) SiBN and (D) SiBCON.

3.3. FT-IR Analysis

FT-IR measurements were performed to provide further evidence for SiBN and SiB-CON. Figure 2A also shows the FT-IR spectra of SiBN at about 1500 cm^{-1} corresponding to the vibrations of C=N and C=C. SiBCON was about 1640 cm^{-1} with C=O vibrations, but acetic acid exhibited the characteristic carbon dioxide peak at 1755 cm^{-1} and 1703 cm^{-1} .

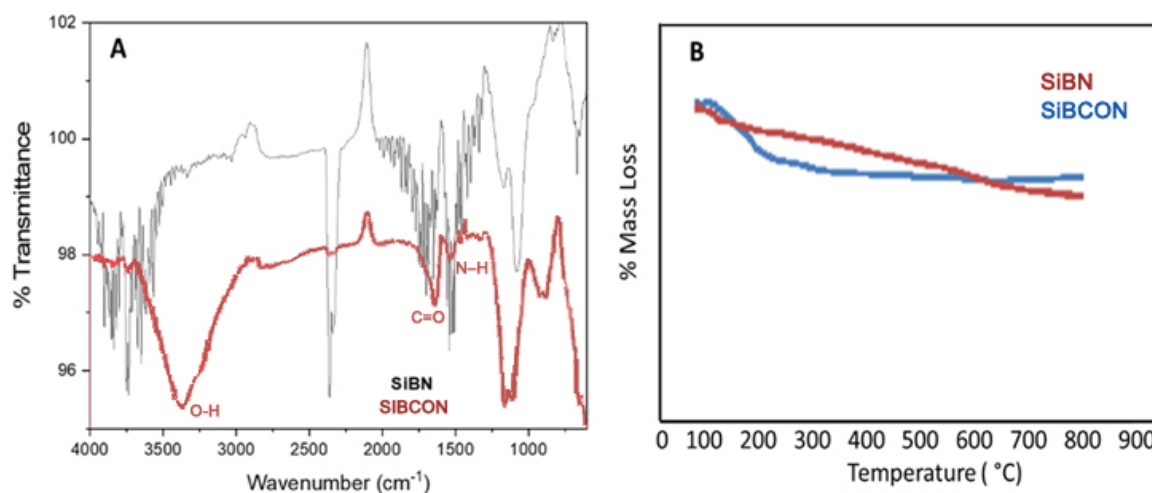


Figure 2. (A) FT-IR spectrum and (B) TGA analysis of SiBN and SiBCON.

3.4. TGA Analysis

Throughout the study, N_2 ($10\text{ }^\circ\text{C min}^{-1}$) was used for thermogravimetric analysis. The results demonstrate that SiBN is stable and exhibits no weight loss at temperatures less than $600\text{ }^\circ\text{C}$; however, SiBCON exhibits weight loss at temperatures about $170\text{ }^\circ\text{C}$. This demonstrates the presence of a functional group (Figure 2B).

3.5. Adsorption Study

3.5.1. Effect of Contact Time

The contact time required between adsorbent/adsorbate to allow direct and dynamic contact for the saturation state was investigated. It is critical to predict the contact time required for optimum CBZ removal, because this provides information about the kinetics of the adsorption reaction and how quickly the process occurs. This was achieved by dissolving 0.02 g of adsorbent in 10 mL of 10 ppm initial concentration of CBZ solution with no pH modifying at room temperature then taking a sample to analyze each period (5, 10, 15, 20, 25, and 30 min). The measurement was made on HPLC instrument; Figure 3 shows the effect of contact time on CBZ removal. As shown in the graph, 15 min was the best time for CBZ removal using SiBN and SiBCON, with adsorption increasing from 45.88% to 74.36% and 40.85% to 72.86%, respectively, and no further high effect on CBZ concentration with additional contact time. Thus, for the two adsorbents, 15 min is the best contact time (Figure 3A).

3.5.2. Effect of pH

The pH of the solution highly affected the adsorption process; therefore, it was an important parameter to study. This was achieved by plotting the percentage removal of CBZ as a function of pH to find at which pH value the maximum adsorption occurred. pH has been studied (2–11), by taking 0.02 g of adsorbent with 10 mL of 10 ppm of adsorbate initial concentration at room temperature, considering the optimum time required. It was clear that the reaction favored the alkaline medium at a high pH value of both adsorbents (SiBN and SiBCON) and the removal ratio increased sharply between 4 and 8, then increased further until it reached pH 9; then, there was no longer an increase in adsorption (Figure 3B). This adsorption favored the alkaline medium as the removal was raised from 55.96% and

53.87% at pH 2 to 89.84% and 88.89% at pH 9, respectively; for further studies, pH 9 was chosen as the optimum parameter.

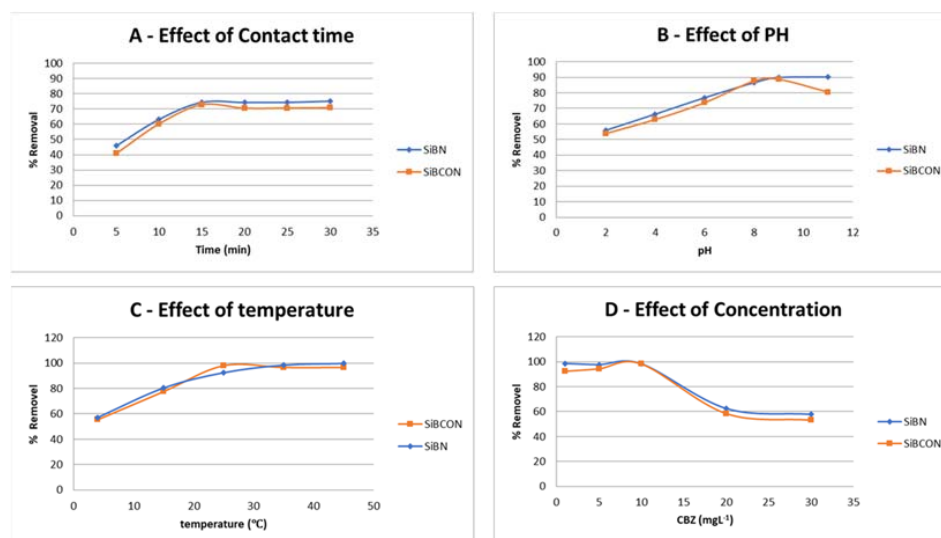


Figure 3. Effect of the removal of CBZ (A) contact time; (B) pH; (C) temperature and (D) CBZ concentration using SiBN and SiBCON.

3.5.3. Effect of Temperature

The optimal conditions for other parameters were considered while studying the influence of temperature on the removal effectiveness of CBZ when utilizing the two adsorbents, SiBN and SiBCON. In general, when the temperature rises, the adsorption effectiveness rises as well. As demonstrated in Figure 3C, the adsorption of CBZ when the two adsorbents (SiBN and SiBCON) were used increased as the temperatures rose from 4 °C to 35 °C and 4 °C to 25 °C, respectively; then, the efficiency of removal remained constant with further increases in temperature, such that the percentage removal of CBZ at the optimum temperature was 98.37% in SiBN and 97.98% in SiBCON, then remained nearly constant, with the high temperature of the solutions increasing the adsorption efficiency, indicating endothermic processes at 35 °C for SiBN and 25 °C for SiBCON which were taken as the optimum temperatures in further tests for the adsorption of CBZ.

3.5.4. Effect of Initial Concentration

The adsorbent has a maximum adsorption capacity for CBZ due to its limited adsorption sites on its surface; there is a suitable initial concentration to start with, to achieve the optimum removal as a high percentage of removal by plotting it as a function of the initial concentration of CBZ. This was accomplished by using 10 mL of 5 different starting concentrations of CBZ standard solution (1, 5, 10, 20, 30 mg·L⁻¹) and treatment for 15 min at (25 °C) with a constant adsorbent dosage of 0.02 g (pH 9). The percentage removal decreased as the starting concentration increased from 2 to 10 mg·L⁻¹. The maximum removal was taken as 98.37% for SiBN and 98.22% for SiBCON at the initial concentration of 10 mg·L⁻¹, even though it was still constant for the lower concentrations (1 and 5 mg·L⁻¹), whereas it was just 57.84% for SiBN and 53.21% for SiBCON in the 30 mg·L⁻¹ solution (Figure 3D).

3.5.5. Kinetic Models and Adsorption Isotherms

Adsorption of CBZ on SiBN and SiBCON followed the mechanism of a pseudo-second-order kinetic model, because the R values in this kinetic model are approximately 1, as shown in Figure 4. The kinetic parameters of the pseudo-(first/second)-order and IPD kinetic models of CBZ adsorption on SiBN, SiBCON, and Figure 4 are shown in the table below. As shown in Figure 4, and as stated in Table 1, the predicted q_e for the pseudo-

second-order tar absorbers is extremely close to the experimental value. When compared with the spurious first-order modeling, the second-order modeling provided a satisfactory match with adsorption.

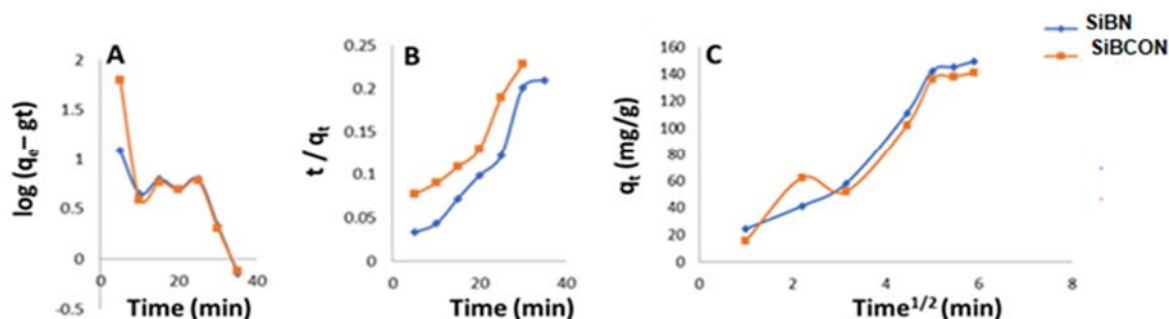


Figure 4. (A) Pseudo-first-order kinetic; (B) pseudo-second-order kinetic and (C) intraparticle diffusion for the adsorption of CBZ.

Table 1. Pseudo-first/second-order and intraparticle diffusion models.

Adsorbents	Adsorption Kinetic Models									
	Pseudo-First-Order				Pseudo-Second-Order			IPD		
	q_e EXP.	q_e (mg/g)	K_1 ($\text{mg}\cdot\text{g}^{-1}\cdot\text{min}^{-0.5}$)	R^2	q_e (mg/g)	K_2 ($\text{mg}\cdot\text{g}^{-1}\cdot\text{min}^{-1}$)	R^2	Z (mg/g)	K_{id} ($\text{mg}\cdot\text{g}^{-1}\cdot\text{min}^{-0.5}$)	R^2
SIBN	148	78	0.14	0.70	148	1.86	0.99	-16.29	28.81	0.95
SIBCON	141	98	0.12	0.69	143	1.52	0.099	-11.065	26.58	0.93

3.5.6. Equilibrium Modeling

The Langmuir and Freundlich isotherms (Figure 5A,B) are most often employed to depict equilibrium data for CBZ adsorption on three adsorbents studied at 25 °C for 30 min with an adsorbent weight of 30 $\text{mg}\cdot\text{L}^{-1}$. The equilibrium research was carried out to elucidate the mechanism of the adsorption process, such as that proposed by Langmuir and Freundlich, who postulated the adsorption of adsorbate as a function of equilibrium concentration. The Langmuir isotherm best depicts the monolayer adsorption of a solute from solution onto an adsorbent surface with a limited number of active sites. Equation (6) depicts the linear version of the Langmuir isotherm model. Table 2 displays the findings of the models. Using Equation (13), a dimensionless constant, R_L , was computed.

$$R_L = \frac{1}{(1 + K_L C_0)} \quad (13)$$

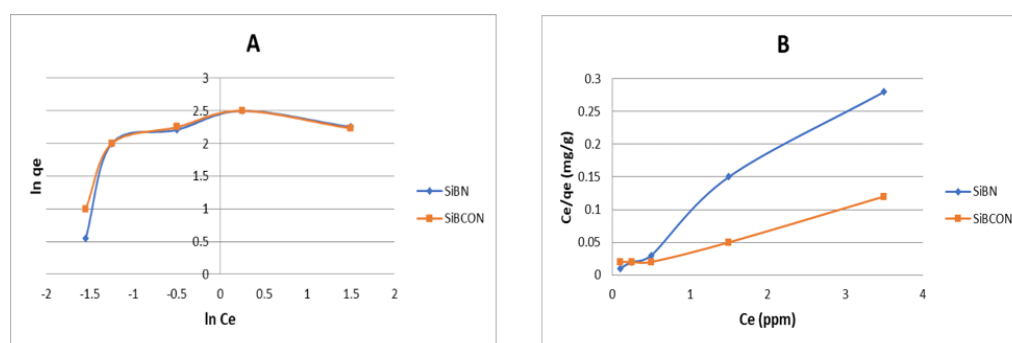


Figure 5. Isotherm models for the remediation of CBZ using (A) Freundlich and (B) Langmuir models.

Table 2. Langmuir and Freundlich models for the CBZ adsorption onto three adsorbents.

Adsorbents	Equilibrium Isotherm Models							
	Langmuir Isotherm			Freundlich Isotherm				
	Q_0 (mg/g)	K_L (L/mg)	R^2	R_L	K_F (mg/g)	$1/n$ (Lg ⁻¹)	n (g/L)	R^2
SiBN	12.78	12.22	0.983	0.45	8.414	0.34	2.93	0.52
SiBCON	18.45	4.9	0.996	0.67	8.302	0.33	2.952	0.52

C_0 is the initial concentration, K_L is the constant linked to adsorption energy (Langmuir constant); the R_L value shows the isotherm shape to be unfavorable if $R_L > 1$, linear if $R_L = 1$, favorable if $0 < R_L < 1$, or irreversible if ($R_L = 0$). The Freundlich isotherm considers the heterogeneous surface and non-uniform heat of sorption distribution. It is most used to describe the multilayer adsorption process (Equation (7)). R^2 has values of approximately 1 when manufactured as a Langmuir model, which indicates that the adsorption of CBZ on three adsorbents is related to the adsorption of Langmuir, as shown in Table 2.

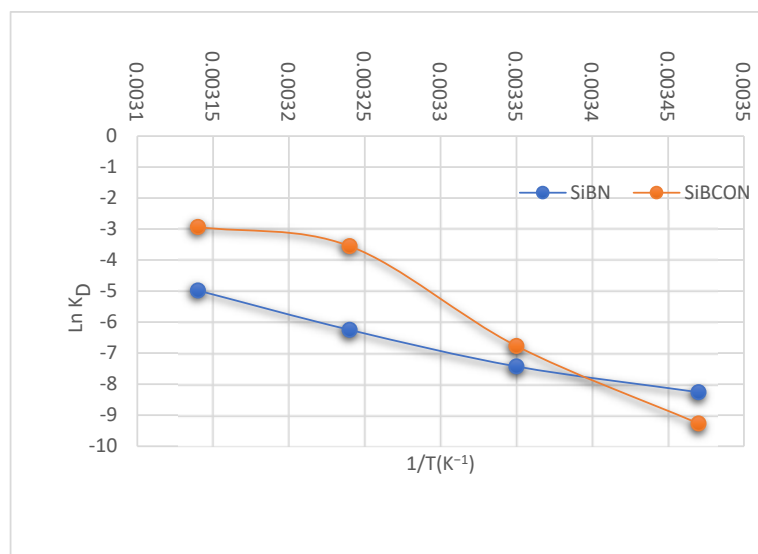
3.6. Thermodynamic Study

As shown in Table 2, the adsorption of CBZ on SiBN and SiBCON is an endothermic process ($\Delta H > 0$), which gives a high percentage of removal with increasing temperature, as well as spontaneously ($\Delta G < 0$). Moreover, both processes tend towards more chaos because the entropy coefficient has a positive value ($\Delta S > 0$).

Table 3 and Figure 6 show the adsorption thermodynamics for the adsorption of CBZ. The adsorbents had negative ΔH values of 82.85 and 169.10 kJ·mol⁻¹ for SiBN and SiBCON, respectively, indicating that the adsorption is endothermic. Positive ΔS values for CBZ on SiBN and SiBCON indicated some order on adsorbent surfaces. Meanwhile, the reaction's spontaneous sorption character was indicated by negative values of ΔG , i.e., -18.18 and -16.82 kJmol⁻¹, for CBZ on SiBN and SiBCON, respectively.

Table 3. Thermodynamics for the adsorption of CBZ at 25 °C.

Adsorbents	Adsorption Thermodynamic		
	ΔH (KJ)	ΔS (J/K)	ΔG (25 °C) (KJ)
SiBN	82.85	217.46	-18.18
SiBCON	169.10	511.24	-16.82

**Figure 6.** Van't Hoff plot for the adsorption of carbamazepine on SiBN and SiBCON.

3.7. Theoretical Calculation

Molecular models of both adsorbents (SiBN and SiBCON) and CBZ are presented in Figure 7A–I. Their calculated properties are collated in Table 4. We optimized four different initial configurations for each adsorbent (SiBN and SiBCON) with carbamazepine. Binding energies E_b were calculated via the following equation:

$$E_b = E(\text{CBZ}) + E(\text{adsorbent}) - E(\text{complex}) \quad (14)$$

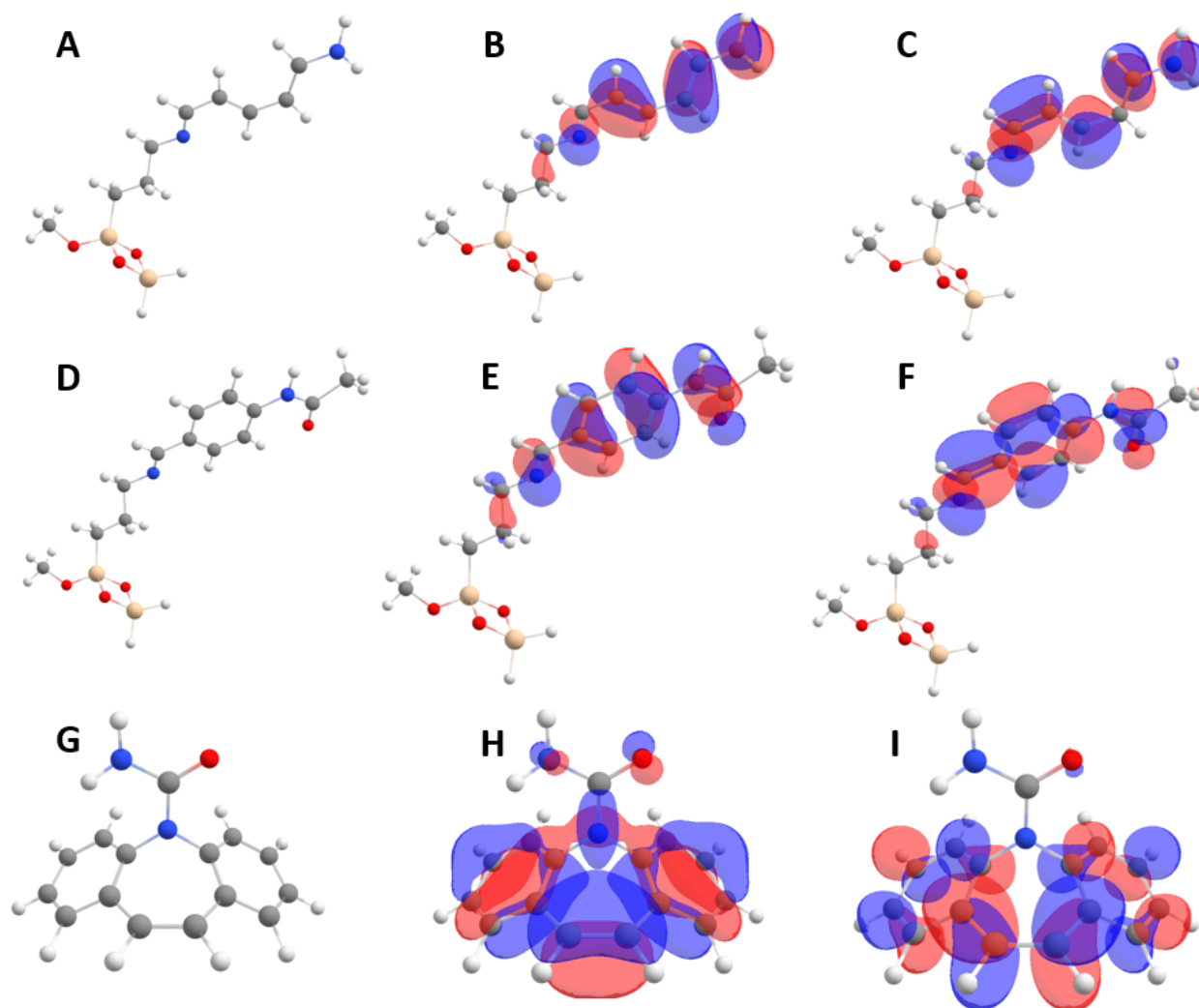


Figure 7. (A) Structure; (B) HOMO and (C) LUMO orbitals for the SiBN molecular model; (D) Structure; (E) HOMO and (F) LUMO orbitals for the SiBCON molecular model; (G) Structure; (H) HOMO and (I) LUMO orbitals for CBZ. Grey, white, blue, red and yellow balls represent carbon, hydrogen, oxygen, nitrogen and silicon atoms, respectively.

Table 4. Calculated properties of adsorbents (SiBN and SiBCON) and CBZ. Dipole moments are presented with/without the inclusion of PCM surface charges.

System	HOMO (eV)	LUMO (eV)	Gap (eV)	χ (eV)	η (eV)	w (eV)	D (Debye)
SiBN	−5.12	−1.39	3.73	3.25	1.86	2.84	8.01/0.35
SiBCON	−6.11	−1.43	4.68	3.77	2.34	3.03	8.25/0.47
CBZ	−6.10	−1.60	4.50	3.85	2.25	3.29	5.33/0.18
SiBN + CBZ	0.41	−4.81	−1.49	3.15	1.66	2.98	5.92/0.19
SiBCON + CBZ	0.59	−5.80	−1.48	3.64	2.16	3.06	8.55/0.33

The most stable complexes with the highest binding energies were selected. Their structures and properties are presented in Figure 8A–F and Table 4. Quantum descriptors provides predictions of the strength of interactions between CBZ and both adsorbates. Chemical hardness provides important hints for highlighting the nature of the reactions [48,49].

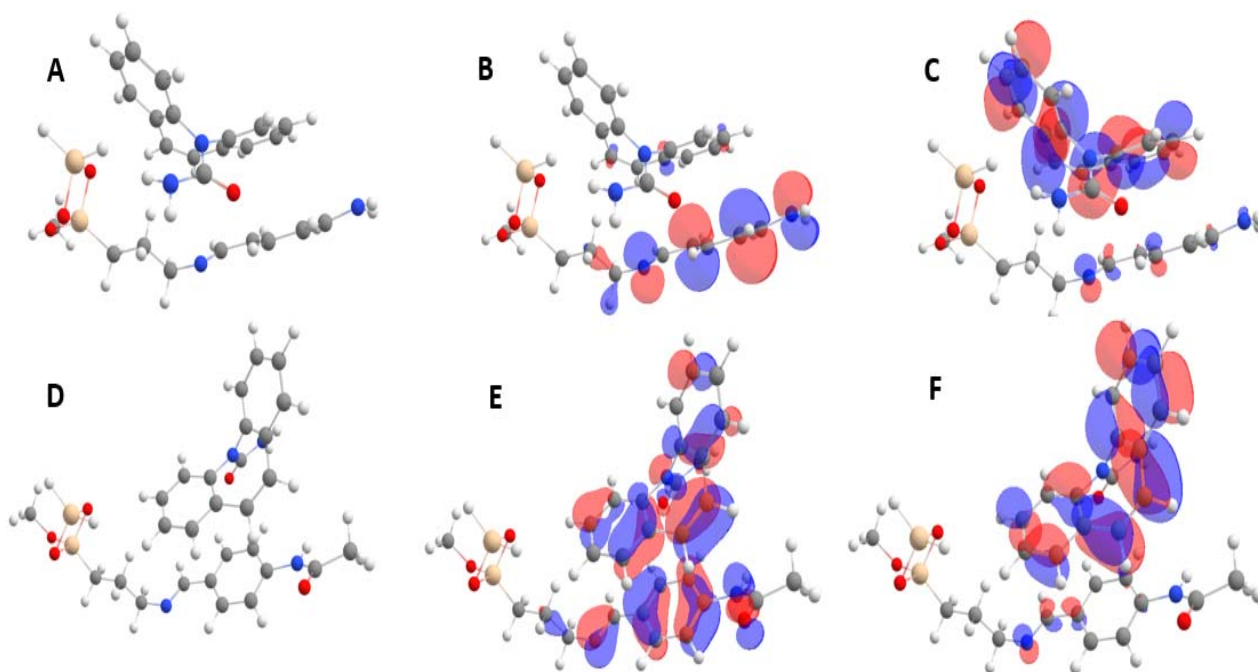


Figure 8. (A) Structure; (B) HOMO and (C) LUMO orbitals for the SiBN+CBZ complex. Structure (D) Structure; (E) HOMO and (F) LUMO orbitals for the SiBCON+CBZ complex. Grey, white, blue, red and yellow balls represent carbon, hydrogen, oxygen, nitrogen and silicon atoms, respectively.

A high hardness indicates the resistance of the molecule against the polarization of electronic clouds. There is an inverse relationship between the hardness and polarization, which showed that the ductility (the multiplicative inverse of stiffness) is proportional to the cube root of polarizability [50]. The hard and soft acid–base principle (HSAB) states that “hard acids prefer to coordinate to hard bases and soft acids prefer to coordinate to soft bases” [51,52]. This means that the mutual compatibility of the molecules is quite important in terms of obtaining a strong interaction.

The chemical hardness values of SiBCON and carbamazepine are quite close to each other. The second principle of the electronic architecture proposed around the concept of stiffness is the maximum hardness principle (MHP) [48,50,51,53]. It is apparent from Table 4 that the SiBCON + CBZ system is harder compared with the SiBN + CBZ system. This observation also supports the power of the interaction between SiBCON and carbamazepine. Another method of predicting the interaction between chemical systems is to calculate the binding energies.

High binding energies are important for explaining the nature of chemical interactions. The calculated binding energies for SiBCON + CBZ and SiBN + CBZ systems are 0.59 and 0.41 eV, respectively. Therefore, HSAB, MHP and the calculated binding energies confirmed that SiBCON interacts with CBZ more strongly than SiBN. This conclusion is consistent with the experimental observations.

4. Conclusions

The preparation of silica-based adsorbents has piqued the interest of many researchers in recent years due to their remarkably wide surface area, homogenous pore structure, and well-modified surface properties. Furthermore, once the adsorption is saturated, it can be repeated several times. Functional silica with SiBN and SiBCON reversed the result for the

adsorption of CBZ and were highly efficient, because both had good adsorption capacity and the rate of removal was increased under optimum conditions: (1) room temperature, (2) pH 9.0, (3) 10.0 ppm initial concentration, and (4) contact time of 15 min. Thus, it can be used as an ideal adsorbent of CBZ from wastewater. Another important feature of those adsorbents, SiBN and SiBCON, is that the adsorption process is an endothermic process ($\Delta H > 0$), which gives a high percentage of removal with increasing temperature, as well as spontaneously ($\Delta G < 0$), which makes them novel to be used in hot areas. Moreover, both processes tend towards more chaos because the entropy coefficient has positive values ($\Delta S > 0$). The results showed that all adsorption processes followed the Langmuir temperature, and all were favorable ($1 > R_L > 0$). The mechanism of all interactions followed the pseudo-kinetic adsorption class II model. Regarding thermodynamics, the parameters showed that all processes are endothermic ($\Delta H > 0$), favorable and spontaneous ($\Delta G < 0$), and the processes reveal a random increase ($\Delta S < 0$), providing the accumulation of CBZ.

Author Contributions: Conceptualization, M.A., S.J. and G.H.; methodology, G.H., I.A., S.R., S.J., R.A. and S.K.; formal analysis, M.A., S.J., J.S., R.A., S.R. and K.P.K.; investigation, M.A., S.T., S.J. and G.H.; resources, M.A., S.J., K.P.K. and S.S.; writing—original draft preparation, M.A. and S.J.; writing—review and editing, M.A. and S.J.; supervision, M.A. and S.J. All authors have read and agreed to the published version of the manuscript.

Funding: The authors would like to thank the Middle East Desalination Research and Center (MEDR_2018_317) managed by the Palestine Water Authority for their financial help during this study.

Institutional Review Board Statement: Not applicable.

Informed Consent Statement: Not applicable.

Data Availability Statement: Not applicable.

Conflicts of Interest: The authors declare no conflict of interest.

References

1. Weber, F.A.; Aus der Beek, T.; Bergman, A.; Carius, A.; Grüttner, G.; Hickmann, S.; Ebert, I.; Hein, A.; Küster, A.; Rose, J.; et al. *Pharmaceuticals in the Environment the Global Perspective: Occurrence, Effects, and Potential Cooperative Action under SAICM*; IWW Rheinisch-Westfaelisches Institut für Wasser, Muelheim an der Ruhr; German Environment Agency: Berlin, Germany, 2016; p. 12.
2. Abdel-Shafy, H.; Mansour, M.S.M. Issue of Pharmaceutical Compounds in Water and Wastewater: Sources, Impact, and Elimination. *Egypt. J. Chem.* **2013**, *566*, 449–471. [[CrossRef](#)]
3. Adams, E.N.; Marks, A.; Lizer, M.H. Carbamazepine-induced hyperammonemia. *Am. J. Health-Syst. Pharm.* **2009**, *66*, 1468–1470. [[CrossRef](#)] [[PubMed](#)]
4. Nevitt, S.J.; Marson, A.G.; Tudur-Smith, C. Carbamazepine versus phenytoin monotherapy for epilepsy: An individual participant data review. *Cochrane Database Syst. Rev.* **2019**, *7*. [[CrossRef](#)] [[PubMed](#)]
5. Oropesa, A.L.; Floro, A.M.; Palma, P. Assessment of the effects of the carbamazepine on the endogenous endocrine system of *Daphnia magna*. *Environ. Sci. Pollut. Res.* **2016**, *23*, 17311–17321. [[CrossRef](#)] [[PubMed](#)]
6. Martín-Díaz, L.; Franzellitti, S.; Buratti, S.; Valbonesi, P.; Capuzzo, A.; Fabbri, E. Effects of environmental concentrations of the antiepileptic drug carbamazepine on biomarkers and cAMP-mediated cell signaling in the mussel *Mytilus galloprovincialis*. *Aquat. Toxicol.* **2009**, *94*, 177–185. [[CrossRef](#)] [[PubMed](#)]
7. Mohapatra, D.P.; Brar, S.K.; Dagherir, R.; Tyagi, R.D.; Picard, P.; Surampalli, R.Y.; Drogui, P. Photocatalytic degradation of carbamazepine in wastewater by using a new class of whey-stabilized nanocrystalline TiO₂ and ZnO. *Sci. Total Environ.* **2014**, *485*, 263–269. [[CrossRef](#)]
8. Scheytt, T.; Mersmann, P.; Lindstädt, R.; Heberer, T. 1-Octanol/water partition coefficients of 5 pharmaceuticals from human medical care: Carbamazepine, clofibrac acid, diclofenac, ibuprofen, and propyphenazone. *Water Air Soil Pollut.* **2005**, *165*, 3–11. [[CrossRef](#)]
9. Zhang, Y.; Geißen, S.U.; Gal, C. Carbamazepine, and diclofenac: Removal in wastewater treatment plants and occurrence in water bodies. *Chemosphere* **2008**, *731*, 151–161. [[CrossRef](#)]
10. Azizollah, N.; Koushali, S.E.; Divsar, F. Synthesis of polypyrrole-chitosan magnetic nanocomposite for the removal of carbamazepine from wastewater: Adsorption isotherm and kinetic study. *J. Environ. Chem. Engin.* **2021**, *9*, 105648. [[CrossRef](#)]
11. Fent, K. Effects of pharmaceuticals on aquatic organisms. In *Pharmaceuticals in the Environment: Sources, Fate, Effects and Risks*; Kümmerer, K., Ed.; Springer: Berlin/Heidelberg, Germany, 2008; pp. 175–203. [[CrossRef](#)]

12. Kebede, T.; Dube, S.; Nindi, M.M. Removal of non-steroidal anti-inflammatory drugs (NSAIDs) and carbamazepine from wastewater using water-soluble protein extracted from *Moringa stenopetala* seeds. *J. Environ. Chem. Eng.* **2018**, *6*, 3095–3103. [[CrossRef](#)]
13. Rajendran, K.; Sen, S. Adsorptive removal of carbamazepine using biosynthesized hematite nanoparticles. *Environ. Nanotechnol. Monitor. Manag.* **2018**, *9*, 122–127. [[CrossRef](#)]
14. Akpınar, I.; Yazaydin, A.O. Rapid and Efficient Removal of Carbamazepine from Water by UiO-67. *Ind. Eng. Chem. Res.* **2011**, *56*, 15122–15130. [[CrossRef](#)]
15. Dwivedi, K.; Morone, A.; Chakrabarti, T.; Pandey, A. Evaluation and optimization of Fenton pretreatment integrated with granulated activated carbon (GAC) filtration for carbamazepine removal from complex wastewater of pharmaceutical industry. *J. Environ. Chem. Eng.* **2018**, *6*, 3681–3689. [[CrossRef](#)]
16. Liu, K.; Yu, J.C.; Dong, H.; Wu, J.C.S.; Hoffmann, M.R. Degradation and mineralization of carbamazepine using an electro-Fenton reaction catalyzed by magnetite nanoparticles fixed on an electrocatalytic carbon fiber textile cathode. *Environ. Sci. Technol.* **2018**, *52*, 12667–12674. [[CrossRef](#)] [[PubMed](#)]
17. McDowell, D.C.; Huber, M.M.; Wagner, M.; von Gunten, U.; Ternes, T.A. Ozonation of Carbamazepine in Drinking Water: Identification and Kinetic Study of Major Oxidation Products. *Environ. Sci. Technol.* **2005**, *39*, 8014–8022. [[CrossRef](#)]
18. Aguilar, C.; Vazquez-Arenas, J.; Castillo-Araiza, O.; Rodríguez, J.L.; Chairez, I.; Salinas, E.; Poznyak, T. Improving ozonation to remove carbamazepine through ozone-assisted catalysis using different NiO concentrations. *Environ. Sci. Pollut. Res.* **2020**, *27*, 22184–22194. [[CrossRef](#)]
19. Ren, Z.; Chen, S.; Jiang, S.F.; Hu, W.F.; Jiang, H. High-efficiency, and ground-state atomic oxygen-dominant photodegradation of carbamazepine by coupling chlorine and g-C₃N₄. *Ind. Eng. Chem. Res.* **2012**, *60*, 2112–2122. [[CrossRef](#)]
20. Chong, M.N.; Jin, B. Photocatalytic treatment of high concentration carbamazepine in synthetic hospital wastewater. *J. Hazard. Mater.* **2012**, *199–200*, 135–142. [[CrossRef](#)]
21. Suriyanon, N.; Punyapalakul, P.; Ngamcharussrivichai, C. Mechanistic study of diclofenac and carbamazepine adsorption on functionalized silica-based porous materials. *Chem. Eng. J.* **2013**, *214*, 208–218. [[CrossRef](#)]
22. Price, P.M.; Clark, J.H.; Macquarrie, D.J. Modified silicas for clean technology. *J. Chem. Soc. Dalton Trans.* **2000**, 101–110. [[CrossRef](#)]
23. Walcarius, A.; Etienne, M.; Lebeau, B. Rate of access to the binding sites in organically modified silicates. 2. Ordered mesoporous silicas grafted with amine or thiol groups. *Chem. Mater.* **2003**, *15*, 2161–2173. [[CrossRef](#)]
24. Grigoropoulou, G.; Stathi, P.; Karakassides, M.A.; Louloudi, M.; Deligibiannakis, Y. Functionalized SiO₂ with N-, S-containing ligands for Pb(II) and Cd(II) adsorption. *Colloids Surf.* **2008**, *320*, 25–35. [[CrossRef](#)]
25. Fan, J.; Wu, C.; Peng, C.; Peng, P. Preparation of xylenol orange functionalized silica gel as a selective solid phase extractor and application for preconcentration-separation of mercury from waters. *J. Hazard. Mater.* **2007**, *145*, 323–330. [[CrossRef](#)] [[PubMed](#)]
26. Shimizu, I.; Yoshino, A.; Okabayashi, H.; Nishio, E.; O'Connor, C.J. Kinetic studies of interaction of 3-aminopropyltriethoxysilane on a silica gel surface using elemental analysis and diffuse reflectance infrared Fourier transform spectra. *J. Chem. Soc. Faraday Trans.* **1997**, *93*, 1971–1979. [[CrossRef](#)]
27. Calisto, V.; Domingues, M.R.M.; Erny, G.L.; Esteves, V.I. Direct photodegradation of carbamazepine followed by micellar electrokinetic chromatography and mass spectrometry. *Water Res.* **2011**, *45*, 1095–1104. [[CrossRef](#)]
28. Metcalfe, C.D.; Koenig, B.G.; Bennie, D.T.; Servos, M.; Ternes, T.A.; Hirsch, R. Occurrence of neutral and acidic drugs in the effluents of Canadian sewage treatment plants. *Environ. Toxicol. Chem. Int. J.* **2003**, *22*, 2872–2880. [[CrossRef](#)]
29. Kajjumba, G.W.; Emik, S.; Öngen, A.; Özcan, H.K.; Aydın, S. *Modelling of Adsorption Kinetic Processes-Errors, Theory and Application, Advanced Sorption Process Applications*; Edebalı, S., Ed.; IntechOpen: Istanbul, Turkey, 2018. [[CrossRef](#)]
30. Sahoo, T.R.; Prelot, B. *Nanomaterials for the Detection and Removal of Wastewater Pollutants*; Elsevier: Amsterdam, The Netherlands, 2020.
31. Zahra, B.A.A.A. Water crisis in Palestine. *Desalination* **2001**, *136*, 93–99. [[CrossRef](#)]
32. Massad, Y.; Hanbali, G.; Jodeh, S.; Hamed, O.; Bzour, M.; Dagdag, O.; Samhan, S. The efficiency of removal of organophosphorus malathion pesticide using functionalized multi-walled carbon nanotube: Impact of dissolved organic matter (DOM). *Sep. Sci. Technol.* **2022**, *57*, 1–12. [[CrossRef](#)]
33. Chakraborty, D.; Chattaraj, P.K. Conceptual density functional theory based electronic structure principles. *Chem. Sci.* **2021**, *12*, 6264–6279. [[CrossRef](#)]
34. Islam, N.; Kaya, S. (Eds.) *Conceptual Density Functional Theory and Its Application in the Chemical Domain*; CRC Press: Boca Raton, FL, USA, 2018.
35. Serdaroglu, G.; Kaya, S.; Touir, R. Eco-friendly sodium gluconate and trisodium citrate inhibitors for low carbon steel in simulated cooling water system: Theoretical study and molecular dynamic simulations. *J. Mol. Liq.* **2020**, *319*, 114108. [[CrossRef](#)]
36. Koopmans, T. Über die Zuordnung von Wellenfunktionen und Eigenwerten zu den einzelnen Elektronen eines Atoms. *Physica* **1934**, *1*, 104–113. [[CrossRef](#)]
37. Krishnan, R.; Binkley, J.S.; Seeger, R.; Pople, J.A. Self-consistent molecular orbital methods. XX. A basis set for correlated wave functions. *J. Chem. Phys.* **1980**, *72*, 650–654. [[CrossRef](#)]
38. Lee, C.; Yang, W.; Parr, R.G. Development of the Colle-Salvetti correlation-energy formula into a functional of the electron density. *Phys. Rev. B* **1988**, *37*, 785–789. [[CrossRef](#)]
39. Becke, A.D. Density-functional thermochemistry. III. The role of exact exchange. *J. Chem. Phys.* **1993**, *98*, 5648–5652. [[CrossRef](#)]

40. Dołęga, A.; Juszyńska-Gałązka, E.; Deptuch, F.; Zieliński, P.M. Thermoanalytical studies of a cytotoxic derivative of carbamazepine: Iminostilbene. *J. Therm. Anal. Calorim.* **2021**, *146*, 2151–2160. [[CrossRef](#)]
41. Wang, L.; Lu, W.; Ni, D.; Xu, T.; Li, N.; Zhu, Z.; Chen, H.; Chen, W. Solar-initiated photocatalytic degradation of carbamazepine on excited-state hexadecachlorophthalocyanine in the presence of peroxymonosulfate. *Chem. Eng. J.* **2017**, *330*, 625–634. [[CrossRef](#)]
42. Katin, K.P.; Grishakov, K.S.; Gimaldinova, M.A.; Maslov, M.M. Silicon rebirth: Ab initio prediction of metallic sp³-hybridized silicon allotropes. *Comput. Mater. Sci.* **2020**, *174*, 109480. [[CrossRef](#)]
43. Xu, H.; Gao, Y.; Liu, Z.; Bei, Y. Theoretical investigation of the hydrolytic mechanism of α -functionalized alkoxy silanes as effective crosslinkers and the difficulty of deep vulcanization in RTV silicone rubber. *Materials* **2018**, *11*, 1526. [[CrossRef](#)]
44. Schmidt, M.W.; Baldrige, K.K.; Boatz, J.A.; Elbert, S.T.; Gordon, M.K.; Jensen, J.H.; Koseki, S.; Matsunaga, N.; Nguyen, K.A.; Su, S.; et al. General atomic and molecular electronic structure system. *J. Comput. Chem.* **1993**, *14*, 1347–1363. [[CrossRef](#)]
45. Pereira da Silva, P.S.; Martín-Ramos, P.; Domingos, S.R.; Bota de Sousa, M.C.; Arranja, C.T.; Sobral, A.J.F.N.; Ramos Silva, M. On the Performance of Hybrid Functionals for Non-linear Optical Properties and Electronic Excitations in Chiral Molecular Crystals: The Case of Butterfly-Shaped Dicinnamalacetone. *ChemPhysChem* **2018**, *19*, 82–92. [[CrossRef](#)]
46. Barrett, E.P.; Joyner, L.G.; Halenda, P.P. The Determination of Pore Volume and Area Distributions in Porous Substances. I. Computations from Nitrogen Isotherms. *J. Am. Chem. Soc.* **1951**, *73*, 373–380. [[CrossRef](#)]
47. Dada, A.; Olalekan, A.; Olatunya, A.; Dada, O. Langmuir, Freundlich, Temkin and Dubinin–Radushkevich isotherms studies of equilibrium sorption of Zn²⁺ unto phosphoric acid modified rice husk. *IOSR J. Appl. Chem.* **2012**, *3*, 38–45.
48. Kaya, S.; Kaya, C.A. A new method for calculation of molecular hardness: A theoretical study. *Comput. Theor. Chem.* **2015**, *1060*, 66–70. [[CrossRef](#)]
49. Kaya, S.; Kaya, C.A. A simple method for the calculation of lattice energies of inorganic ionic crystals based on the chemical hardness. *Inorg. Chem.* **2015**, *54*, 8207–8213. [[CrossRef](#)] [[PubMed](#)]
50. Ghanty, T.K.; Ghosh, S.K. Correlation between hardness, polarizability, and size of atoms, molecules, and clusters. *J. Phys. Chem.* **1993**, *97*, 4951–4953. [[CrossRef](#)]
51. Pearson, R.G. Hard and soft acids, and bases. *J. Am. Chem. Soc.* **1963**, *85*, 3533–3539. [[CrossRef](#)]
52. Louleb, M.; Latrous, L.; Ríos, A.; Zougagh, M.; Rodríguez-Castelloñ, E.; Algarra, M.; Soto, J. Detection of Dopamine in Human Fluids Using N-Doped Carbon Dots, *ACS Appl. Nano Mater.* **2020**, *2*, 8004–8011. [[CrossRef](#)]
53. Kaya, S.; Kaya, C.; Islam, C. Maximum hardness and minimum polarizability principles through lattice energies of ionic compounds. *Phys. B Condens. Matter* **2016**, *485*, 60–66. [[CrossRef](#)]